J Mater Sci: Mater Med (2008) 19:83–93
DOI 10.1007/s10856-007-3046-1

Effect of heat treatment on structure and properties of dispersed-type dental amalgam

Chien-Ping Ju · Yu-Hsuan Chen · Wen-Fu Ho · Shu-Ching Ho · Wen-Cheng Chen · Dar-Bin Shieh · Jiin-Huey Chern Lin

Received: 20 March 2006 / Accepted: 5 May 2006 / Published online: 19 June 2007

Abstract Effect of heat treatment of Ag–Cu–Pd dispersant particles on the structure, mechanical properties and mercury vapor release rate of an Ag–Cu–Sn/Ag–Cu–Pd-based dental amalgam has been investigated. Experimental results indicate that crystallinity of dispersant Ag-Cu–Pd alloy increases with increasing HTT, with most notable increase occurring between 100 and 200 °C. Increasing HTT of Ag–Cu–Pd alloy does not change much of the mercury/alloy ratio for amalgamation, but largely reduces working/setting time of the amalgam. The Ag–Cu–Pd particles in 7 d-aged amalgam are comprised primarily of an outer Sn/Cu/Pd-rich zone and an inner Ag/Cu/Pd-rich zone with eutectic-type morphology and chemical distribution. The annealing-enhanced Pd segregation effect is most significantly observed in the amalgam derived from 300 °C-annealed Ag–Cu–Pd dispersant. This amalgam also has the highest compressive strength, highest DTS, and lowest creep rate. Higher annealing temperature causes mechanical property of the amalgam to deteriorate. The initial mercury vapor release rates of amalgams derived from 100, 200 and 300 °C-annealed Ag–Cu–Pd dispersant are significantly lower than that derived from 400 °C-annealed dispersant.

C.-P. Ju · Y.-H. Chen · W.-F. Ho · S.-C. Ho · W.-C. Chen · J.-H. Chern Lin (✉)
Department of Materials Science and Engineering, National Cheng-Kung University, No. 1, Da-Sha Road, Tainan 701, Taiwan, ROC
e-mail: chernlin@mail.ncku.edu.tw

D.-B. Shieh
Department of Dentistry, Center for Micro/Nano Science and Technology, National Cheng Kung University Medical College, No. 1, Da-Sha Road, Tainan 701, Taiwan, ROC

Introduction

Dental amalgam is popularly used as a direct posterior restorative filling material due to its high strength, durability and wear resistance [1, 2], as well as long-term satisfactory clinical performance [3]. Nevertheless, there is an increasing interest in the study of potential mercury hazard from dental amalgam. Mercury vapor released from newly-placed and aged dental amalgams, including low-copper and high-copper amalgams, has been identified [4–10]. The effects of mercury on human health as well as on environmental pollution remain a major concern among both the scientific community and the general public.

A number of approaches have been proven effective in improving the performance of dental amalgam, including reducing the mercury release rate. For example, encouraging results from dispersed-type dental amalgams containing 0.5–10 wt% Pd in their dispersant alloy phase have been reported in the mid-1980s [11–13]. The Pd-induced improved properties include a drastically reduced early-stage mercury vapor release rate [14, 15] and better corrosion resistance [13], among others.

The effect of particle configuration on the structure and properties of dental amalgam has also been found significant. For example, in their results from four dispersed-type Pd-containing amalgams with the same chemical composition but different particle configurations, Chen et al. [16] indicated that the amalgam fabricated from irregular (lathe-cut) Ag–Cu–Sn matrix and irregular Ag–Cu–Pd dispersant particles had the lowest early-stage mercury vapor release rate. Nevertheless, this amalgam also demonstrated the lowest compressive strength and largest creep rate among four amalgams.

Process conditions are also critical to the performance of dental amalgam. Among many process details, the relief of the process-induced internal stresses from amalgam alloy particles is perhaps the most critical issue. Particularly during manufacturing of irregular-type amalgam particles, the cutting or milling-induced stresses in the particles can cause changes in amalgam alloy properties, such as amalgamation rate and dimensional changes during hardening [17, 18].

Generally the process-induced residual stresses can be relieved by carrying out an annealing treatment at a moderate temperature on the alloy. It was reported that, when milled amalgam alloy was maintained at room temperature, its internal residual stress was relieved over a period of weeks or months [19]. When annealed at 100 °C, this stress-relieving process could be shortened to several hours [20, 21]. Higher annealing temperatures (up to 240 °C) under inert gas atmosphere ($N_2/H_2 =$ 80/20) were also disclosed in the US patent No. 4859412 [22]. In a microstructural study of Ag–Cu–Pd alloy dispersant particles, Chern Lin et al. [23] indicated that the lathe cutting-induced residual stress in the particles, which was accompanied with a phenomenon of X-ray diffraction (XRD) peak broadening, could be largely removed by annealing the alloy particles in argon atmosphere at 90 °C for at least 1 week.

The focus of the present study is to investigate the effects of annealing of Ag–Cu–Pd dispersant particles on the structure, mechanical properties and mercury vapor release rate of a dental amalgam derived from irregularly-shaped Ag–Cu–Sn matrix alloy particles combined with irregularly-shaped Ag–Cu–Pd dispersant particles. Improvement in mechanical properties while maintaining a low early-stage mercury vapor release rate of the amalgam is attempted. The annealing temperature used in the present study, 100–400 °C, is much higher than those reported in the literature.

Materials and methods

The matrix alloy (70wt%Ag-4wt%Cu-26wt%Sn) and dispersant alloy (62wt% Ag-28wt%Cu-10wt%Pd) were prepared from raw materials of 99.99 wt% pure silver, 99.99 wt% pure copper, 99.5 wt% pure palladium and 99.9 wt% pure tin. The irregularly-shaped particles were prepared by melting the desired metals at 1100 °C for 360 min in a quartz tube sealed in argon gas. The furnace-cooled alloy ingot was then homogenized at 800 °C for 480 min.

The homogenized ingot was mounted in a lathe and comminuted into irregularly-shaped particles. The lathe-cut irregular particles were then ball-milled and sieved through #325 mesh into desired sizes (majority less than 45 μm) using a SPEX 8000 ball mill (A.O. Smith Corp., USA). Since a preliminary study of the present authors indicated that 30 min and 65 min were appropriate ball-milling times respectively for lathe-cut Ag–Cu–Sn and Ag–Cu–Pd particles, such ball-milling times were used throughout the present study.

Sieved particles were subjected to various heat treatments under argon gas protection, followed by a pickling treatment in 10% HCl solution for 30 min. Four different temperatures (100, 200, 300 and 400 °C) were selected for the heat treatment of Ag–Cu–Pd particles in this study. The amalgams derived from the Ag–Cu–Pd dispersant particles heat-treated for 48 h at these four temperatures are designated ''PdH10'', ''PdH20'', ''PdH30'' and ''PdH40'', respectively. Since in a preliminary study the phenomenon of sintering started to be observed when the alloy powder was heat-treated to 450 °C or above, the heat treatment temperature (HTT) above 450 °C is avoided in the present study. The preliminary study also indicated that, as Ag–Cu–Sn matrix particles were heat-treated at 400 °C for 24 h, the lowest mercury/alloy ratio was obtained. For this reason, while Ag–Cu–Pd dispersant particles were heat-treated at different temperatures, the heat treatment of Ag–Cu–Sn particles was conducted under such condition (400 °C for 24 h) throughout this study.

Trituration of alloy/mercury mixture was carried out in a closed capsule using a commercial triturator (Crescent LP-60, Lyons, IL, USA). The alloy contained two parts of Ag–Cu–Sn powder and one part of Ag–Cu–Pd powder (by weight). As a result, the alloy had an overall composition of 67.2wt% Ag, 12.0wt% Cu, 17.4wt% Sn, and 3.4wt% Pd. The triturated amalgam mass was hand-condensed in a disk-shaped acrylic die of 10 mm in diameter and 2 mm in depth for phase identification and mercury vapor release measurement.

Phase identification of the series of amalgam was conducted using a Rigaku D-MAX/IIB X-ray diffractometer (Rigaku Corp., Tokyo, Japan) operated at 30 kV and 20 mA. Cu-Kα radiation scanning from 29 to 45° (2θ) at a scanning speed of 0.5°/min was used. The microstructure and chemistry were characterized using a Hitachi S-4200 scanning electron microscope (SEM) equipped with an energy dispersive spectrometer (EDS).

Cylindrical-shaped specimens (4 mm in diameter and 8 mm in height) were used for compressive strength, diametral tensile strength (DTS) and creep tests. The specification of the specimens was complied with ADA Spec. No. 1 for the measurement of mechanical properties of dental amalgams. The compressive strength and DTS of the amalgams were measured using a Shimatzu AGS-500D dynamic mechanical tester (Shimatzu Corp., Kyoto, Japan) at a crosshead speed of 0.5 mm/min. The compressive

strength of each specimen was calculated according to the equation, $P = 4F/\pi D^2$, where P is compressive strength in MPa, F the fracture load in N, and D the diameter of the specimen in mm. The DTS value was calculated according to the equation, $\sigma_t = 2F/\pi Dt$, where σ_t is DTS in MPa, F the fracture load in N, D the diameter of the specimen in mm, and t the specimen thickness in mm. The creep rate of amalgam at 37 °C under a pressure of 36 MPa for 4 h was calculated using the equation, Creep = $(L4\text{-}L_1)/L_0$ x 100%, where L_0 is original length of the specimen in mm, and L_1 and L_4 the lengths after 1 and 4 h, respectively, under the load. All compressive strength, DTS and creep rates are averages of five tests under each condition. One-way ANOVA was used to evaluate data and Scheffé multiple comparison test was run to determine the significance of deviations among each group. In all cases the statistical difference was considered significant at $P < 0.05$ level.

The measurement of mercury vapor release rate was carried out using a Jerome gold film mercury vapor analyzer (JEROME 431–X, Arizona Instrument LLC Phoenix, AZ, USA). Atmospheric-pressure air was blown continuously through the tubing of an aquarium pump at a rate of 750 mL/min which is equal to the air-suction rate of the mercury vapor analyzer. The first reading was taken at 90 s after trituration. After each measurement, the specimen was removed from the detection chamber and clean air was pumped through the analyzer until the reading dropped back to zero to ensure that no mercury vapor was left in the chamber [14].

Results and discussion

Alloy particle morphology and size distribution

The morphology and particle size distribution of ball-milled Ag–Cu–Sn and Ag–Cu–Pd particles used for the study are shown in Fig. 1. Both particles essentially had an irregular shape. Ag–Cu–Sn particles showed a narrower particle size distribution than Ag–Cu–Pd particles. The majority (>90 vol%) of Ag–Cu–Sn particles had sizes ranging from 5 to 30 μm with the largest portion of the particles (>25 vol%) having sizes around 10 μm. The majority (>90 vol%) of Ag–Cu–Pd particles had sizes ranging 10–60 μm with the largest portion (>25 vol%) having sizes about 30 μm. The ball-milling yield of Ag–Cu–Sn particles was found much higher than that of Ag–Cu–Pd, indicating that Ag–Cu–Sn particles were more easily comminuted than Ag–Cu–Pd particles. The lower ball-milling yield of Ag–Cu–Pd dispersant alloy than Ag–Cu–Sn matrix alloy is believed due to the higher content of Cu, which is harder than Sn, in Ag–Cu–Pd than in Ag–Cu–Sn. The final amalgam alloy was comprised of 1/3 (by weight) Ag–Cu–Pd and 2/3 Ag–Cu–Sn.

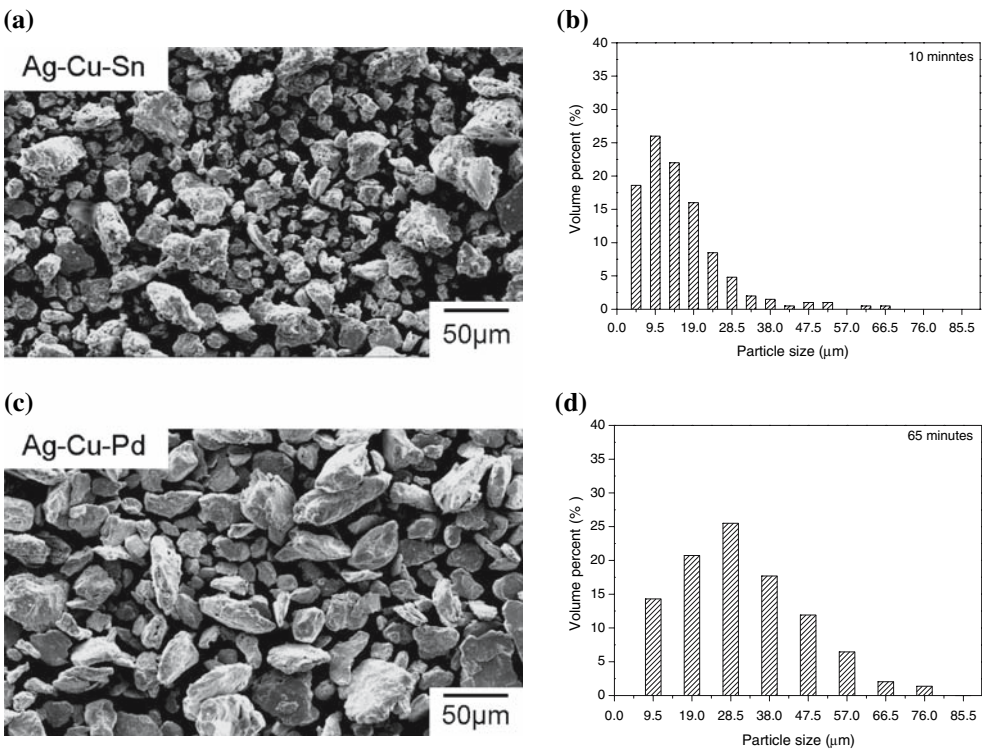

Fig. 1 Morphology and size distribution of Ag–Cu–Sn and Ag–Cu–Pd powders used in this study

Effect of heat treatment on crystallinity of Ag–Cu–Pd dispersant alloy

The XRD patterns of Ag–Cu–Pd dispersant alloy annealed at different temperatures are given in Fig. 2. As shown in the figure, the XRD patterns of annealed dispersant alloy are comprised entirely of Ag and Cu peaks. Whether Cu_3Pd phase is present in the annealed alloy cannot be confirmed by these XRD patterns due to the overlapping of its major peaks with Cu peaks and/or its small quantity.

The relatively broad XRD peaks observed in 100 °C-annealed alloy is believed to be a result of milling-induced residual stresses [23, 24]. The sharpness of XRD peaks, which is an indication of crystallinity of the alloy, was found to increase with increasing HTT. The increase in crystallinity of the dispersant alloy was most significant as HTT increased from 100 to 200 °C, suggesting that milling-induced residual stress has been largely relieved in this temperature range.

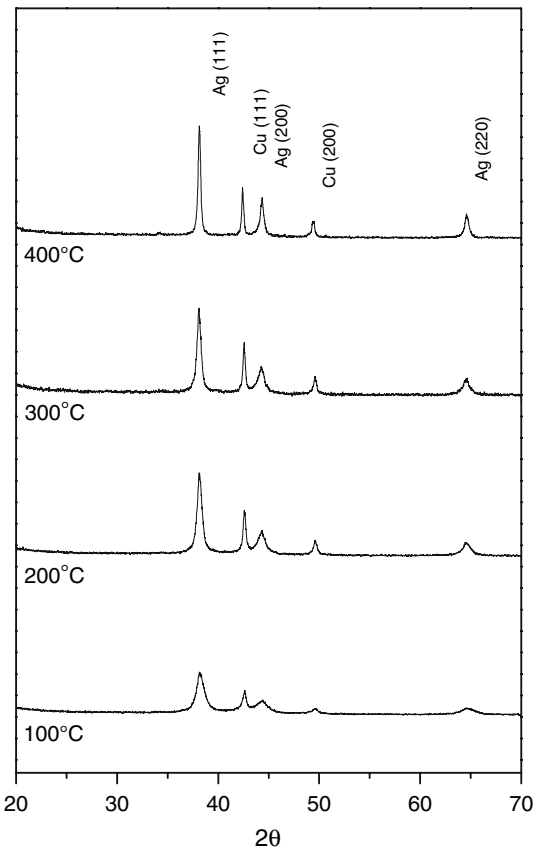

Fig. 2 XRD patterns of Ag–Cu–Pd alloy powders heat-treated at different temperature

Effect of heat treatment on amalgamation reaction

On mercury/alloy ratio and working/setting time

While increasing HTT of Ag–Cu–Pd dispersant alloy did not change much the mercury/alloy ratio for amalgamation, the working and setting times largely reduced from 15 to 7 min and from 25 to 9 min, respectively, as HTT increased from 100 to 400 °C (Table 1). It is generally believed that, in dispersed-type amalgam, Ag–Cu–Sn matrix alloy is the primary component participating in the formation of γ_1 (Ag_2Hg_3) amalgam matrix phase during amalgamation reaction. The fact that working/setting time of the present amalgam was largely reduced by increasing HTT of Ag–Cu–Pd dispersant alloy suggests that dispersant alloy was also effectively involved in amalgamation reaction. The release of milling-induced internal stress by heat-treating Ag–Cu–Pd particles is believed to have an essential effect on accelerating amalgamation reaction and shortening working/setting time [20]. Whether or how much has the later-described ''Pd segregation effect'' contributed to the shortening of working/setting time is not certain at this moment.

On phase transitions

XRD patterns of the four amalgams (derived from Ag–Cu–Pd dispersant annealed to different temperatures) aged at 37 °C for 1 h, 24 h, and 7 days are shown in Fig. 3. Reaction phases such as γ_1 (Ag_2Hg_3) and η' (Cu_6Sn_5), as well as non-reacted γ (Ag_3Sn) phase, were identified in all amalgams. The γ_2 ($Sn_{7-8}Hg$) peaks with moderate intensity were only detected in amalgams aged for 1 h at 37 °C. A delayed amalgamation due to Pd addition, that suppressed the formation of η' and hence promoted the formation of γ_2 phase at the early stage may have caused this result [25]. According to Chen [25], the γ_2 phase could further react with copper from Ag–Cu–Pd and promote the formation of η' phase and thus was diminished itself. In the present study, γ_2 phase was indeed no longer found in amalgams aged for 24 h or longer. The dominance of γ_1 phase over all other phases at 1 h indicates that formation of γ_1 phase was largely completed in a short period of time. The XRD patterns of amalgams aged for 24 h and 7 d are almost identical. Qualitatively the heat treatment does not seem to result in significant differences in XRD patterns among amalgams annealed at different temperatures.

Effect of heat treatment on amalgam microstructure

SEM micrographs and their accompanied EDS elemental maps of the four amalgams aged for 7 days are shown in

Table 1 Mercury/alloy ratio, working and setting time of amalgam with (62%Ag- 28%Cu-10%Pd) dispersant alloys subjected to various heat treatments conditions

Amalgam	Heat treatment temperature and time		Mercury/alloy ratio	Working time (min)	Setting time (min)
	Ag–Cu–Sn	Ag–Cu–Pd			
PdH10	400 °C, 24 h	100 °C, 48 h	1.1	15	25
PdH20	400 °C, 24 h	200 °C, 48 h	1.1	12	18
PdH30	400 °C, 24 h	300 °C, 48 h	1.1	8	12
PdH40	400 °C, 24 h	400 °C, 48 h	1	7	9

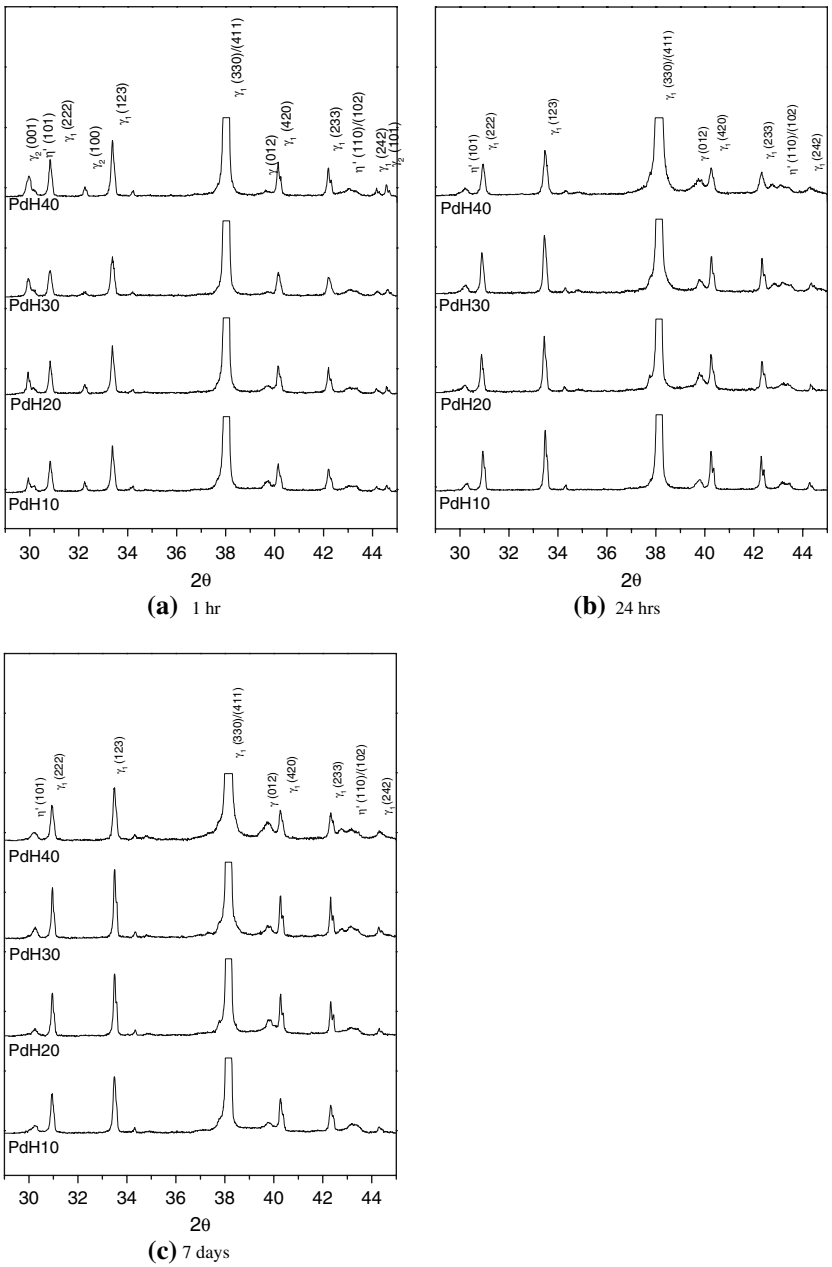

Fig. 3 XRD patterns of amalgams aged for (**a**) 1 h (**b**) 24 h and (**c**) 7 days

Fig. 4. As labeled in the figure, the original Ag–Cu–Sn particles had been largely turned into white-appearing (under secondary electron imaging mode) matrix which is rich in Hg, less rich in Ag, and substantially depleted in other elements. Within the matrix are distributed two types of small particles with different contrasts:

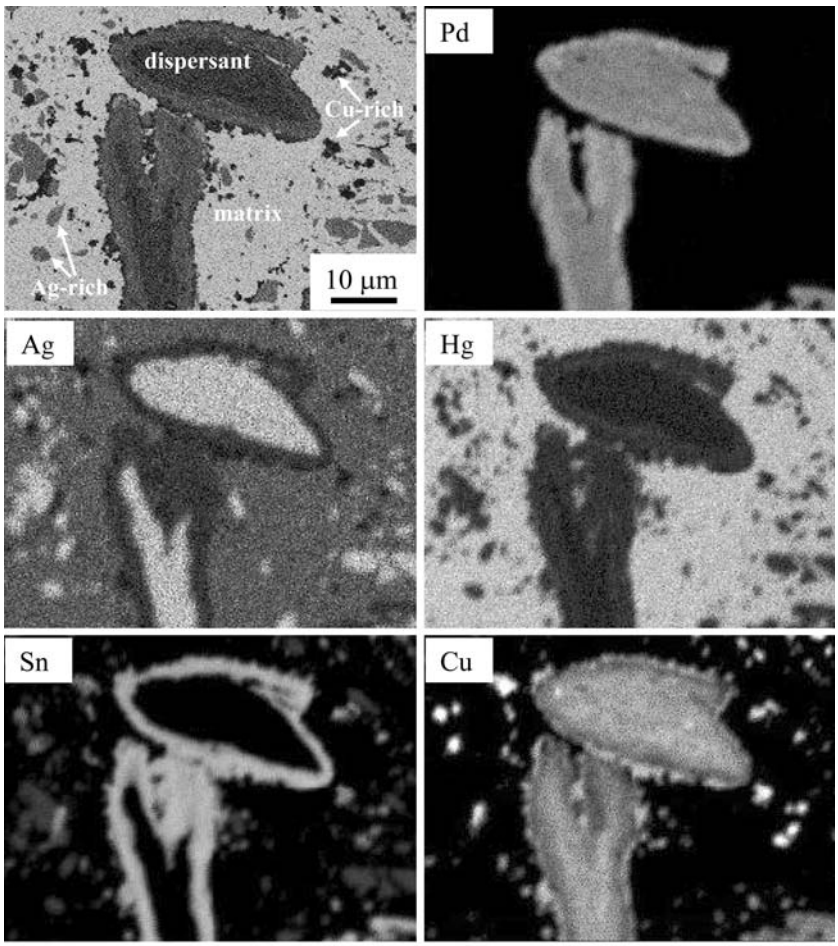

Fig. 4 SEM morphology and EPMA chemical analysis of the amalgams. (**a**) PdH10 (**b**) PdH20 (**c**) PdH30 (**d**) PdH40

(I) gray-appearing particles rich in Ag, less rich in Sn, and substantially depleted in other elements; and (II) dark-appearing particles rich in Cu, less rich in Sn, and substantially depleted in other elements. These gray and dark-appearing particles are believed to be the remaining (non-reacted) Ag_3Sn (γ) and Cu_3Sn (() phases [16, 25], respectively, of the original Ag–Cu–Sn particles.

Although the microstructure of amalgam matrix was not significantly affected by the heat treatment conducted on Ag–Cu–Pd dispersant particles, the microstructure of Ag–Cu–Pd dispersant itself was noticeably affected by the heat treatment. As shown in Fig. 4(a), each Ag–Cu–Pd particle is comprised primarily of two portions with different contrasts under secondary electron imaging mode: (I) darker-appearing inner portion with higher concentrations of Ag, Cu and Pd and lower concentrations of Sn and Hg; and (II) lighter-appearing outer portion with higher concentrations of Sn, Cu and Pd and lower concentrations of Ag and Hg. The high contents of Cu and Sn in the outer portion indicates the possible formation of η' (Cu_6Sn_5) phase in this reaction zone, consistent with the finding of earlier reports [26, 27]. In commercial admixed Cu-rich amalgams, reaction zones containing both η' and γ_1 phases are often found in areas surrounding Ag–Cu dispersant particles [26, 27].

Within the inner Ag/Cu/Pd-rich zone was still observed the eutectic-type morphology of original Ag–Cu–Pd particles. Earlier studies [26, 27] indicate that the darker-appearing component of this lamellar-type morphology is Cu-rich, while the lighter-appearing component is Ag-rich. These studies also indicate that Pd is preferentially segregated into the Cu-rich phase. It is interesting to note that, although the overall concentration of Hg was relatively low in the Ag/Cu/Pd-rich inner zone, its distribution demonstrated a non-uniform, lamellar-type feature. This lamellar-type distribution in the inner zone indicates that a certain degree of amalgamation reaction- most likely between Hg and Ag- has proceeded far inside the inner zone of dispersant particles which is traditionally believed not critically involved in the amalgamation reaction in admixed-type amalgams.

The microstructure of PdH20 amalgam was similar to that of PdH10 amalgam (Fig. 4(b)). When Ag–Cu–Pd particles were heat-treated to 300 °C, however, noticeable

Fig. 4 continued

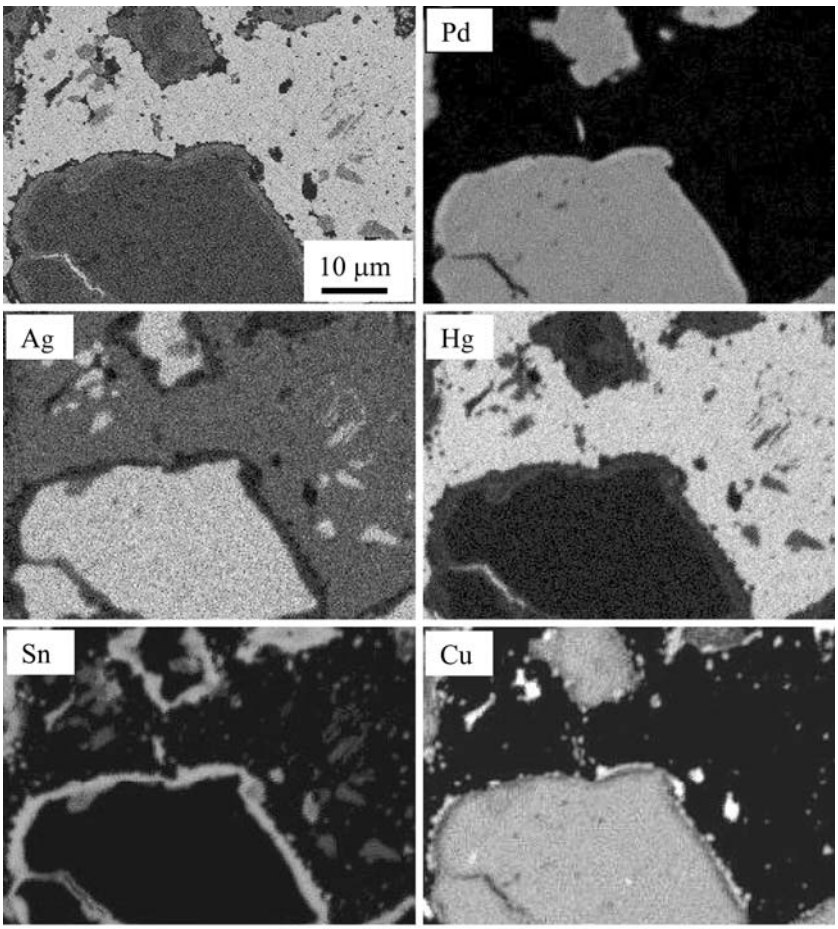

(b) PdH20

changes in its derived amalgam microstructure- particularly in dispersant component- were observed. As shown in Fig. 4(c), not only the same lamellar-type morphology (as mentioned earlier in lower temperature-annealed dispersant particles) was observed throughout the inner zone of dispersant particles, the elemental maps of Cu and Pd also demonstrated a lamellar-type feature. Careful examination of the elemental maps reveals that the elemental distributions in Cu and Pd coincide with each other, reconfirming the earlier finding that Pd is more ''attracted'' to Cu than to Ag in Ag–Cu–Pd dispersant phase [28]. Although whether Cu_3Pd phase was formed during annealing is not sure, as mentioned earlier, the annealing-enhanced segregation of Pd into Cu-rich phase at relatively high temperatures (300 °C or above) is certain. The elemental distribution in Hg, on the other hand, seems unrelated to Cu/Pd distribution.

Furthermore, the concentrations of Cu and Pd in the outer reaction zone of 300 °C-annealed dispersant particles in the amalgam appeared much lower than those annealed at lower temperatures. A possible explanation for the ''disappearance'' of contrasts in the elemental maps of Cu and Pd (especially Cu) in the reaction zone of this amalgam would be the earlier-mentioned annealing-induced preferential ''bond'' between Cu and Pd, which suppresses Cu-Sn reaction and the formation of η' phase.

When Ag–Cu–Pd dispersant particles were annealed at 400 °C, the lamellar-type contrasts in both Cu and Pd maps within dispersant particles became lower than those annealed at 300 °C, indicating a declined Pd segregation effect at 400 °C (Fig. 4(d)). The highest Cu/Pd contrast—indication of the greatest Pd segregation effect-at 300 °C might help explain the later-mentioned optimal amalgam properties at such annealing temperature.

Effect of heat treatment on amalgam mechanical behavior

The compressive strength and DTS of the four amalgams are presented in Figs. 5 and 6, respectively. Except PdH40, all other amalgams had 1 h compressive strengths higher than the ADA requirement (80 MPa). One-way ANOVA statistical analysis indicated that the 1 h compressive strength of PdH30 amalgam (123 MPa) was significantly

Fig. 4 continued

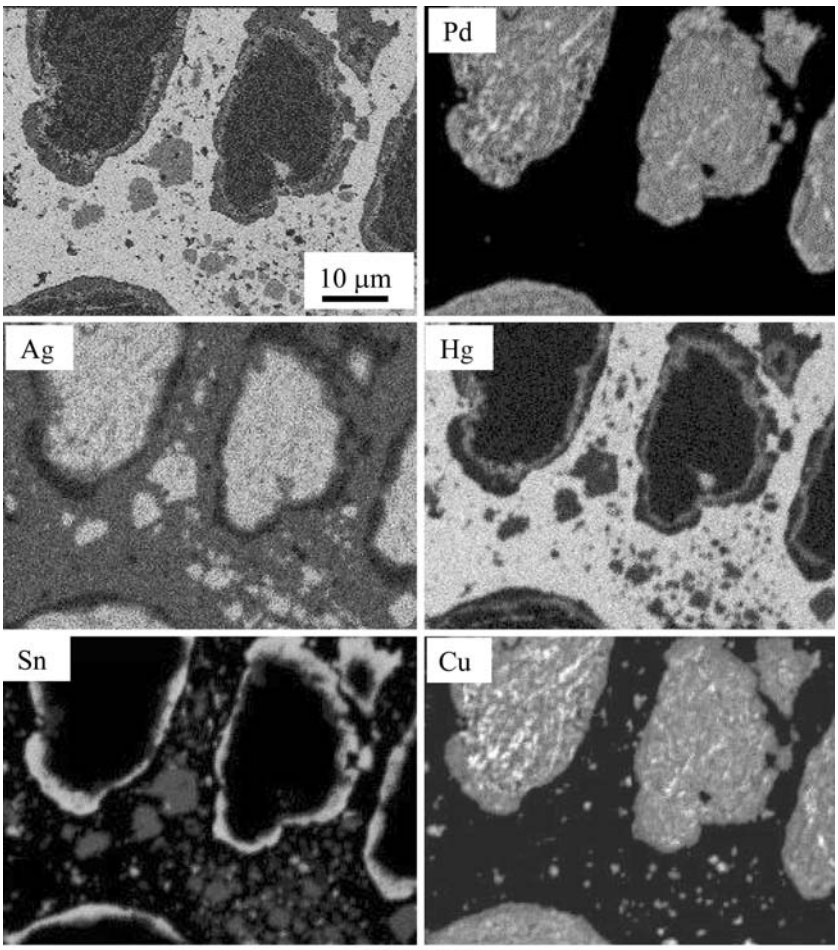

(c) PdH30

($P < 0.001$) higher than other three amalgams. Further increase in annealing temperature to 400 °C caused the compressive strength to decline. The variation in 24 h compressive strength with annealing temperature followed the same trend. The PdH30 amalgam had the highest 24 h compressive strength. Further increase in annealing temperature also caused the 24 h compressive strength to decline. The 1 h and 24 h DTS values of PdH30 amalgam were also higher than all other amalgams, as shown in Fig. 6. Again, ''overheating'' (to 400 °C) of Ag–Cu–Pd dispersant particles caused the DTS of the amalgam to decrease.

Creep is considered one major factor contributing to the marginal deterioration of dental amalgam [29, 30] and a reasonable indicator of clinical marginal fracture of amalgam restorations [31]. The creep rates of all present amalgams were lower than ADA requirement (≤3%). The heat treatment effect on creep resistance of the amalgam followed the same trend as on compressive strength. As indicated in Fig. 7, the creep rate of the amalgam decreased with increasing annealing temperature until reaching the lowest value (1.03%) at 300 °C. This creep rate is smaller than that annealed at 100 °C (PdH10) by as much as 1.80 %. Again, further increase in annealing temperature (to 400 °C) caused the creep resistance to decline.

Although the measurement of such mechanical properties as compressive strength, DTS and creep of amalgam is straightforward, the interpretation of the data could be quite complicated. In general, such effects as relative amounts of various phases, microstructure/morphology, porosity level and availability of stress-concentrated sites could all influence the mechanical properties of amalgam. According to Osborn et al. [32], the amalgamation rate could also influence amalgam mechanical properties, especially early strength. In the present study, the working and setting times continued to decrease with increasing HTT of Ag–Cu–Pd dispersant (Table 1). This shortened working/setting time (an accelerated amalgamation reaction) may have contributed to the observed optimal mechanical properties of PdH30 amalgam. On the other hand, the enhanced amalgamation reaction cannot explain the deterioration in mechanical performance of PdH40 amalgam. The observed partial sintering among Ag–Cu–Pd

Fig. 4 continued

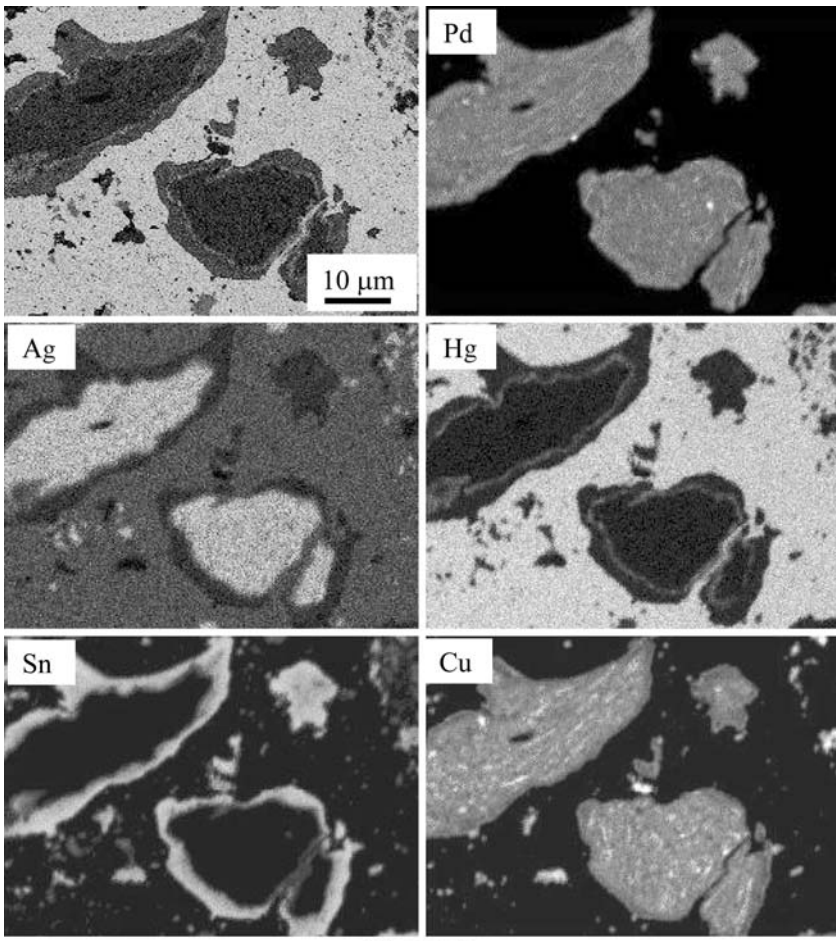

(d) PdH40

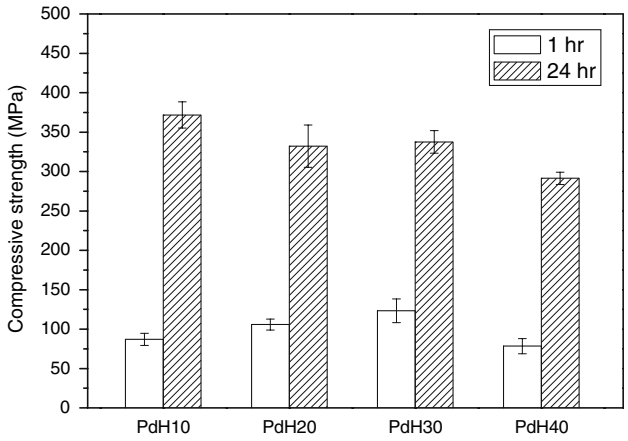

Fig. 5 1 h and 24 h compressive strengths of amalgams

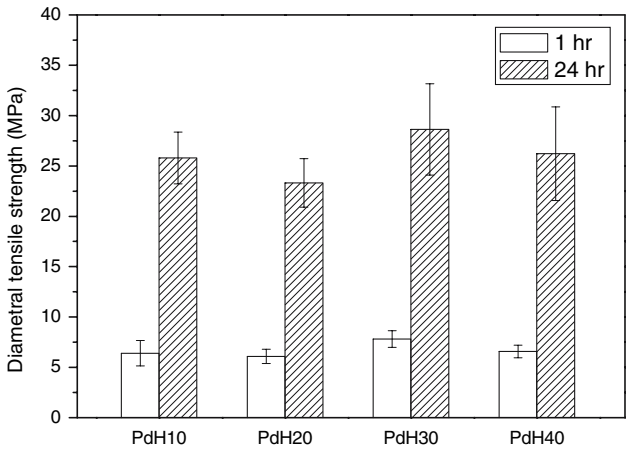

Fig. 6 1 h and 24 h diametral tensile strengths of amalgams

particles at 400 °C might help explain the deteriorated mechanical performance of PdH40.

Another worth-noting factor that may affect the performance of the present amalgam would be the annealing-enhanced segregation of Pd into Cu-rich phase at relatively high temperatures. As mentioned earlier, the highest Cu/Pd contrast, which is an indication of the largest Pd segregation effect, was observed in PdH30 amalgam. The best mechanical performance was also found in this amalgam.

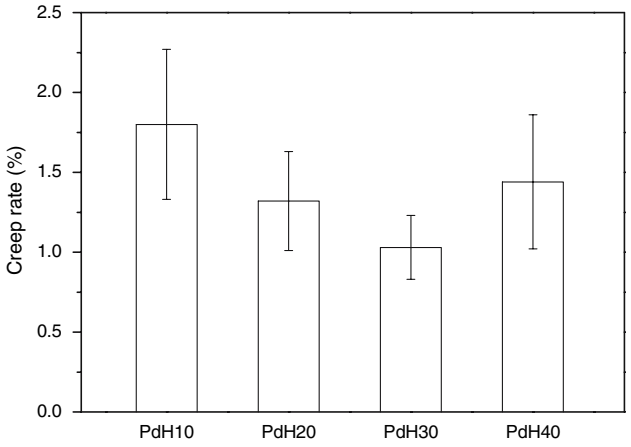

Fig. 7 Compressive creep rates of amalgams aged for 7 days

Effect of heat treatment on amalgam mercury release rate

The effect of heat treatment on initial mercury vapor release rate of the amalgam is demonstrated in Fig. 8. The initial mercury vapor release rates of amalgams derived from Ag–Cu–Pd dispersant annealed at 100, 200 and 300 °C were all in the range between 20 and 30 pg/mm^2 s. One-way ANOVA statistical analysis indicated that the initial mercury vapor release rate of PdH40 amalgam derived (36 pg/mm^2 s) was significantly ($P < 0.001$) higher than other three amalgams. Neither annealing-induced acceleration in amalgamation reaction nor segregation of Pd into Cu-rich phase can satisfactorily interpret this much higher mercury release rate observed in PdH40 amalgam. Whether the earlier-mentioned partial sintering effect at such high temperature has played a role in the determination of initial mercury vapor release rate of the present amalgam is not clear at this moment. The mercury release rate of each amalgam quickly dropped with incubation time

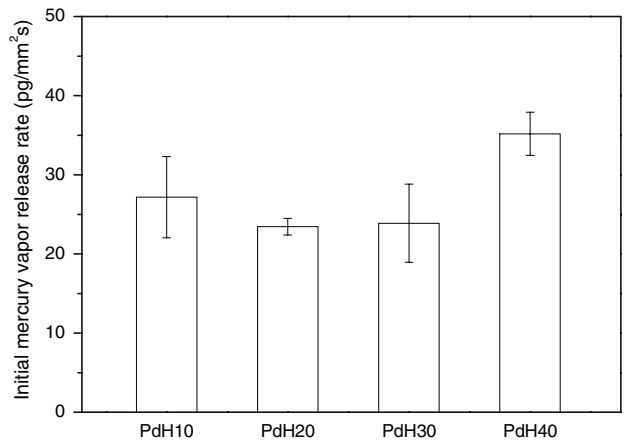

Fig. 8 Initial mercury vapor release rates of amalgams

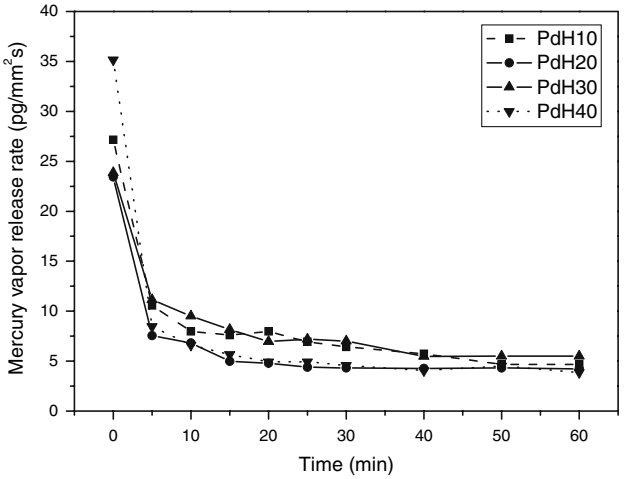

Fig. 9 Early stage mercury vapor release rates of amalgams

and reached a plateau value of 5–8 pg/mm^2 s after 15 min (Fig. 9) as a result of surface oxidation which slowed down further release of mercury [6, 29].

Conclusions

1. The XRD patterns of annealed Ag–Cu–Pd dispersant alloy are comprised entirely of Ag and Cu peaks. Crystallinity of the alloy increases with increasing HTT, with most notable increase occurring between 100 and 200 °C.
2. Increasing HTT of Ag–Cu–Pd dispersant alloy does not much change mercury/alloy ratio for amalgamation, but largely reduces working/setting time of the amalgam.
3. The Ag–Cu–Pd dispersant particles of amalgam aged for 7 days are comprised primarily of a Sn/Cu/Pd-rich outer zone and an Ag/Cu/Pd-rich inner zone with eutectic-type morphology and chemical distribution. The annealing-enhanced segregation of Pd into Cu-rich phase is most significantly observed in the amalgam derived from 300 °C-annealed Ag–Cu–Pd dispersant.
4. The amalgam derived from 300 °C-annealed Ag–Cu–Pd dispersant has the highest compressive strength, highest DTS, and lowest creep rate. Further increase in annealing temperature causes amalgam mechanical performance to deteriorate.
5. The initial mercury vapor release rates of amalgams derived from 100, 200 and 300 °C-annealed Ag–Cu–Pd dispersant (20–30 pg/mm^2 s) are significantly lower than that derived from 400 °C-annealed dispersant (36 pg/mm^2 s). The mercury release rates of all amalgams drop with incubation time and reach a plateau value of 5–8 pg/mm^2 s after a short period of time.

Acknowledgements This investigation was supported in part from the National Health Research Institute (NHRI) of the Republic of China under Contract No. NHRI-EX93-9317EI.

References

1. A. LUSSI, M. BRUNNER, P. PORTMANN and W. BÜERGIN, *Eur. J. Oral Sci.* **103** (1995) 388
2. D. S. MOORE, W. W. JOHNSON and I. KAPLAN, *Int. J. Prosthodont* **8** (1995) 461
3. E. BJERTNESS and T. SONJU, *Acta. Odontol. Scand.* **48** (1990) 93
4. K. C. CHAN and C. W. SVARE, *J. Dent. Res.* **51** (1972) 555
5. C. W. SVARE, C. W. FRANK and K. C. CHAN, *J. Dent. Res.* **52** (1972) 740
6. L. V. POWELL, G. H. JOHNSON and D. J. BALES, *J. Dent. Res.* **68** (1989) 1231
7. T. OKABE, *Dent. Mater.* **3** (1987) 1
8. T. OKABE, J. FERRACANE, C. COOPER, H. MATSUMOTO and M. WAGNER, *J. Dent. Res.* **66** (1987) 33
9. T. OKABE, T. YAMASHITA, I. NAKAJIMA, A. BERGLUND, L. ZHAO, I. GUO and J. L. FERRACANE, *J. Dent. Res.* **73** (1994) 1711
10. J. L. FERRACANE, T. HANAWA and T. OKABE, *J. Dent. Res.* **71** (1992) 1151
11. E. H. GREENER and K. H. CHUNG, *J. Dent. Res.* **61** (1982) 1192
12. E. H. GREENER, K. H. CHUNG and J. H. CHERN LIN, *Biomaterials* **9** (1988) 213
13. P. COLON, N. PRADELLE-PLASSE and J. GALLAND, *Dent. Mater.* **19** (2003) 232
14. J. H. CHERN LIN, H. C. LEE and C. P. JU, *Biomaterials* **18** (1997) 1
15. T. OKABE, K. OHMOTO, H. NAKAJIMA, M. WOLDU and J. L. FERRACANE, *J. Dent. Mater.* **16** (1997) 191
16. K. I. CHEN, J. H. CHERN LIN and C. P. JU, *Biomaterials* **20** (1999) 1851
17. A. GREASLEY and D. L. BAKER, *J. Brit. Dent.* **144** (1978) 303
18. R. W. PHILLIPS, *Sinners science of dental materials* (W. B. Saunders Co., Philadelphia, 1982) p. 302–329
19. R. G. CRAIG, *Restorative dental materials* (C. V. Mosby Co., St. Louis, Missouri, 1989) p. 231
20. K. J. ANUSAVICE, *Phillips' science of dental materials* (W. B. Saunders Co., Philadelphia, 1996) p. 366
21. M. R. CHODKOWSKI, US Patent No. 4664629, 1987
22. W. GROLL, D. HATHAWAY and G. SCHOCK, US Patent No. 4859412, 1989
23. J. H. CHERN LIN, K. H. CHUNG and E. H. GREENER, *Dent. Mater.* (1992) **8**, 85
24. M. M. A. VRIJHOEF, *J. Biomed. Mater. Res.* **11** (1977) 339
25. K. I. CHEN, J. H. CHERN LIN and C. P. JU, *J. Dent. Res.* **75** (1996) 1497
26. R. W. BRYANT, *J. Oral Rehab.* **12** (1985) 27
27. R. W. BRYANT, *J. Oral Rehab.* **12** (1985) 37
28. J. H. CHERN LIN and E. H. GREENER, *Dent. Mater.* **7** (1991) 254
29. J. W. OSBORNE, E. N. GALE, C. L. CHEW, B. F. RHODES and R. W. PHILLIPS, *J. Dent. Res.* **57** (1978) 983
30. D. B. MAHLER, *J. Dent. Res.* **59** (1980) 1420
31. D. B. MAHLER, L. G. TERKLA, J. VAN EYSDEN and M. H. REISBICK, *J. Den. Res.* **49** (1970) 1452
32. J. W. OSBORNE and T. G. BERRY, *Oper. Dent.* **20** (1995) 26